J Mater Sci (2010) 45:1478–1486
DOI 10.1007/s10853-009-4106-3

Synthesis and characterization of mesoporous silica/poly(*N*-isopropylacrylamide) functional hybrid useful for drug delivery

Andreza de Sousa · Daniel Andrada Maria · Ricardo Geraldo de Sousa · Edésia Martins Barros de Sousa

Received: 14 August 2009 / Accepted: 9 November 2009 / Published online: 22 December 2009

Abstract Recent studies indicate the use of mesoporous silica and polymeric sensitive hydrogels as suitable for drug delivery systems due to their specific characteristics. Polymeric hydrogels, such as poly(*N*-isopropylacrylamide) [P(*N*-iPAAm)], show volumetric expansion/contraction behaviour at 306 K, which that can be used to develop a thermosensitive drug delivery system. In this study, we report a facile and direct synthesis route to obtain hybrid functional nanosystems based on silica-P(*N*-iPAAm) by using a neutral surfactant and without any functionalization method and the assessment of its release rate of a model drug. The materials were characterized by Fourier transform infrared spectroscopy, nitrogen adsorption, scanning electron microscopy, transmission electron microscopy and thermal analysis. A release assay with atenolol monitored by UV–Vis spectroscopy was performed for pure SBA-15 and a hybrid system at different temperatures in order to evaluate the influence of the thermosensitive behaviour of the polymer on the release kinetics. The response of the hybrid system as a drug delivery device is influenced by the volumetric contraction of P(*N*-iPAAm) up to the lower critical solution temperature (LCST) due to phase transition. Above the LCST, drug release depends essentially on the temperature.

A. de Sousa · D. A. Maria · E. M. B. de Sousa (✉)
Serviço de Nanotecnologia—Centro de Desenvolvimento da Tecnologia Nuclear CDTN/CNEN, Avenida Presidente Antônio Carlos, 6.627—Campus da UFMG—Pampulha, CEP 31270-90 Belo Horizonte, Minas Gerais, Brazil
e-mail: sousaem@cdtn.br

A. de Sousa · R. G. de Sousa
Departamento de Engenharia Química, E.E.UFMG, Avenida Presidente Antônio Carlos, 6.627—Campus da UFMG—Pampulha, CEP 31270-90 Belo Horizonte, Minas Gerais, Brazil

Introduction

In the last decade, significant research efforts were devoted to obtaining materials with well-defined nanostructures for a wide range of applications [1–4]. Mesoporous materials currently are a field of intensive activity due to their high potential in a very broad range of applications, since they offer not only tunable acid strength and well-defined pore diameters, but also more accessible active sites than microporous zeolites do [5–7]. A series of inorganic mesostructured materials, such as MCM41, HMS, SBAn and so on, has been synthesized with different templating schemes [8–10]. These mesoporous materials can be used as medical devices due to their large pores and well-defined structure. Mesoporous silica derived from triblock copolymers, such as SBA-15, is suggested to have a potential to act as a convenient reservoir for controlled drug delivery systems due to their large pore, high hydrothermal stability and easy preparation [11]. Nevertheless, mesoporous systems present a major problem as far as drug release is concerned—limited control of its drug release, which occurs mainly by diffusion. The need to develop new materials with optimal tailored characteristics has spurred a growing interest in hybrid materials, especially organic and inorganic nanocomposites.

Temperature-responsive hydrogels, such as poly(*N*-isopropylacrylamide) [P(*N*-iPAAm)], are a well-studied class of drug delivery systems, as they can respond pronouncedly to temperature changes [12, 13]. In water, P(*N*-iPAAm) exhibits phase transition at a lower critical solution temperature (LCST) of approximately 306 K [14]. Below the LCST, the hydrogel incorporates water and swells, whereas the release of water in response to an increase in temperature causes shrinkage. The swelling and shrinkage of this gel upon temperature changes is of

interest for controlled release of molecules, such as medicines [15].

Hybrid functional nanosystems based on silica-P(*N*-iPAAm) have attracted much attention for control of molecular transport, including drug release, because self-regulated delivery allows for drug release when it is needed. You et al. [16] presented P(*N*-iPAAm)-modified micro-to-mesoporous silica nanoparticles with sizes in the order of 100 nm synthesized by chemical attachment of a preformed polymer to prepare porous particles. Temperature-dependent uptake and release of small molecules by porous silica nanoparticles was achieved by treating preformed, thiol-functionalized micro-to-mesoporous silica nanoparticles with pyridyl disulphide-terminated (P(*N*-iPAAm)-S-S-Py). The design of a delivery system based on stimulus-responsive P(*N*-iPAAm) inside a mesostructured cellular foam via atom transfer radical polymerization was reported by Zhou et al. [17], who investigated the control of drug release in response to environmental temperature. Zhu et al. [18] reported a novel synthesis of a multi-functional delivery system based on ordered mesoporous silica SBA-15 with magnetic particles formed in situ and thermo-sensitive P(*N*-iPAAm). They employed hydrophilic $FeCl_2$ as an additional precursor to fabricate magnetic particles inside SBA-15 via surfactant template sol–gel process and the polymerization of *N*-iPAAm was implemented inside the pores of SBA-15 with magnetic particles system. However, to our knowledge, most of the previous studies reported the hybrid system synthesis using surface modification. In our point of view, particularly the reported routes had limitations as controlled drug release devices: (a) complex multistep approaches; (b) decreased of the pore size and surface area as a result of the surface functionalization [19]. Such limitations may affect the applicability of these materials as drug delivery systems.

We report a facile and direct synthesis route to obtain silica-P(*N*-iPAAm)-based hybrid functional nanosystems by using a neutral surfactant without any functionalization method and evaluate the release rate of a model drug by this system. To this end, two different materials were used and compared, pure SBA-15 and a hybrid nanosystem. The procedure adopted to incorporate the hydrogel into the SBA-15 network was monomer adsorption followed by in situ polymerization. The hybrid nanosystem was characterized by Fourier transform infrared spectroscopy (FTIR), nitrogen adsorption, scanning electron microscopy (SEM), transmission electron microscopy (TEM) and thermogravimetric analysis (TGA). Additionally, a special continued flow was employed to assay the drug release profile of the system. We studied the influences of the second compound and the temperature on the behaviour of the silica matrix as a controlled drug release device and compared the release kinetics of the model drug (atenolol) from pure SBA-15.

Experimental

Material synthesis

SBA-15 silica was prepared according to Zhao et al. [20] using commercial triblock copolymer Pluronic P123-$PEO_{20}PPO_{70}$-PEO_{20} [poly(ethylene glycol)-block-poly(propylene glycol)-block-poly(ethylene glycol)] (Sigma–Aldrich, St. Louis, MO, USA) as a templating agent. P123 copolymer was dissolved in a mixture of distilled water and HCl under agitation, followed by the addition of tetraethyl orthosilicate. The mixture was maintained at 308 K for 24 h, then for 1 day at 373 K under static conditions in a Teflon-coated autoclave. The obtained material was filtered and dried at 313 K and the surfactant was removed by calcination (823 K for 5 h).

Synthesis of the SBA-15/P(*N*-iPAAm) hybrid

The hybrid was prepared using the following procedure: 0.5 g of calcined SBA-15 was added to 3.5 mL solution of 0.245 g of monomer (*N*-iPAAm) and 0.005 g of crosslinking agent (*N*,*N*,*N*′,*N*′-methylene-bisacrylamide). The mixture was transferred to an INNOVA 4200 (150 rpm) shaker and the mixture was continuously purged with nitrogen. The solution was then allowed to polymerize for 24 h in a water bath at 282 K. The obtained hybrid material was dried at 333 K for 24 h and subsequently washed to remove the excess monomers, crosslinking agent, initiator and accelerator. In the washing stage, the material was disaggregated, suspended in water and continuously stirred. The hybrid was then collected by centrifugation at 3600 rpm for 3 min and dried at 333 K for 24 h. It was designated [SBA-15/P(*N*-iPAAm)] 5 × 1, where 5 × 1 is the gel composition studied [21]. The monomer: SBA-15 mass ratio used was 1:2 (w/w).

Characterization techniques

Methods

Nitrogen adsorption isotherms of samples were obtained at 77 K using a Quantachrome Nova 2200 adsorption analyser. Before the adsorption measurements, SBA-15 and hybrid samples were outgassed for 24 h at 393 and 313 K, respectively, in the degas port of the adsorption analyser. All data analyses were performed using the NovaWin V.10© 1997–2007 Quantachrome Instruments software (Boynton Beach, FL, USA). SEM characterization was

performed in an SEM (JEOL JSM, 840A) operating at 15 kV. TEM characterization was performed through a Tecnai—G2-20-FEI 2006 electron microscope with an acceleration potential of 200 kV. The weight loss of the samples was determined in a Shimadzu thermogravimetric analyser (TGA) 50WS. All measurements were carried out under nitrogen atmosphere (20 mL min^{-1}) using a sample mass of approximately 3 mg from room temperature to 973 K at 283 K min^{-1}. FTIR was performed in an FTIR ABB BOMEN-MB102 using the KBr pellet method in the range 4000–400 cm^{-1}.

Calculations

BET-specific surface area, S_{BET}, was calculated from adsorption data in the relative pressure interval $P/P_0 =$ 0.045–0.25. A cross-sectional area of 0.162 nm^2 was used for the nitrogen molecule in the BET calculations. The total pore volume, V_p, was calculated from the amount of N_2 adsorbed at the highest P/P_0 ($P/P_0 = 0.99$) [22]. The micropore volume, V_μ, of SBA-15 silica was estimated from nitrogen adsorption data using the α_s plot method [23] in the standard reduced adsorption, α_s, interval from 0.75 to 1 (relative pressure range from 0.15 to 0.40). The external surface area, S_{ext}, was evaluated using a α_s interval from 1.6 to 3.0. The primary mesopore volume, V_{meso}, was estimated as the difference between the total pore volume and the micropore volume. The α_s-plot was analysed by the standard reduced adsorption for nonporous hydroxylated silica [24]. The mesopore size distributions were calculated from the adsorption branches of the nitrogen isotherms employing the BJH algorithm.

Drug adsorption and release

SBA-15 was loaded with atenolol as follows: 0.5 g of the powder sample was added to 150 mL of an atenolol solution (10 mg mL^{-1}) and shaken for 48 h at 298 K (200 rpm). A 3:1 weight ratio of atenolol/solid sample was used. Powder atenolol loaded samples were recovered by filtration, washed with distilled water and kept to dry for 24 h at 333 K. The same procedure was used to load the hybrid with atenolol. Small atenolol loaded sample discs with 7-mm diameter and 2-mm thick were obtained under uniaxial pressure (2 MPa for SBA-15 and 3 MPa for the hybrid system). TGA was performed to evaluate the percentage of atenolol adsorbed by each sample. In vitro drug delivery assays were performed in steady-state regime flow conditions by soaking the sample discs into simulated body fluid [11] at 298, 303, 308, and 313 K in permanent regimen flow system with the aid of a peristaltic pump. First, the discs were put into the sample holder and immersed into an ultrathermo bath. The delivered atenolol concentration was monitored by UV spectrometry at 274 nm using a UV–Vis Shimadzu model 2401 spectrometer.

Results and discussion

Material characterization

Table 1 summarizes the textural properties of pure SBA-15 and the [SBA-15/P(*N*-iPAAm)] hybrid. A sensible difference was observed in the values of S_{BET} and S_{ext} of SBA-15 and [SBA-15/P(*N*-iPAAm)], which may be an indication of the presence of polymer in the pore structure of silica. The surface area S_{BET} decreased from 672 to 326 $m^2\ g^{-1}$ (~51%) and S_{ext} from 53 to 13 $m^2\ g^{-1}$ (~75%) after *N*-iPAAm polymerization. The primary mesopore volume and total pore volume of [SBA-15/P(*N*-iPAAm)] (0.42 and 0.48 $cm^3\ g^{-1}$) was lower than the SBA-15 values (0.83 and 0.96 $cm^3\ g^{-1}$), respectively. The pore diameter decreased from 5.70 to 3.76 nm (~34%). However, the atenolol molecule could still easily fit inside the pores of the hybrid material. Analogous pore volume reductions were observed for organic/mesoporous silica hybrid materials with polymer confined in mesopores [16, 25, 26].

The nitrogen adsorption isotherms for pure SBA-15 and the [SBA-15/P(*N*-iPAAm)] hybrid are shown in Fig. 1. In both cases, the isotherms were type IV, according to the IUPAC classification, which is associated with the presence of mesopores [22]. SBA-15 has similar and nearly parallel adsorption and desorption branches, with a H1-type hysteresis loop, which is characteristic of uniform mesopores with open cylindrical geometry. After the formation of P(*N*-iPAAm) in the SBA-15 network, a symmetric reduction in hysteresis was observed. This reduction occurred mainly in the desorption branch. The analysis of the isotherms and the respective adsorption and desorption-derived curves (Fig. 1) reveal a reduction in symmetry and the occurrence of a stepwise desorption phenomenon in the hybrid sample, suggesting bimodal porosity. Kruk et al. [27] attributed this stepwise desorption phenomenon due to the presence of constrictions in the porous structures. According to the authors, in the case of a pore connected to neighbouring pores or its the surroundings through entrances (constrictions) with diameter smaller than the pore diameter, capillary evaporation from the pore interior

Table 1 N_2 adsorption results

Sample	S_{BET}	S_{ext}	V_{meso}	V_{micro}	V_{BJH}	D_{BJH}
SBA15	672	53.0	0.830	0.0200	0.956	5.70
[SBA-15/P(*N*-iPAAm)]	326	13.0	0.420	0	0.484	3.76

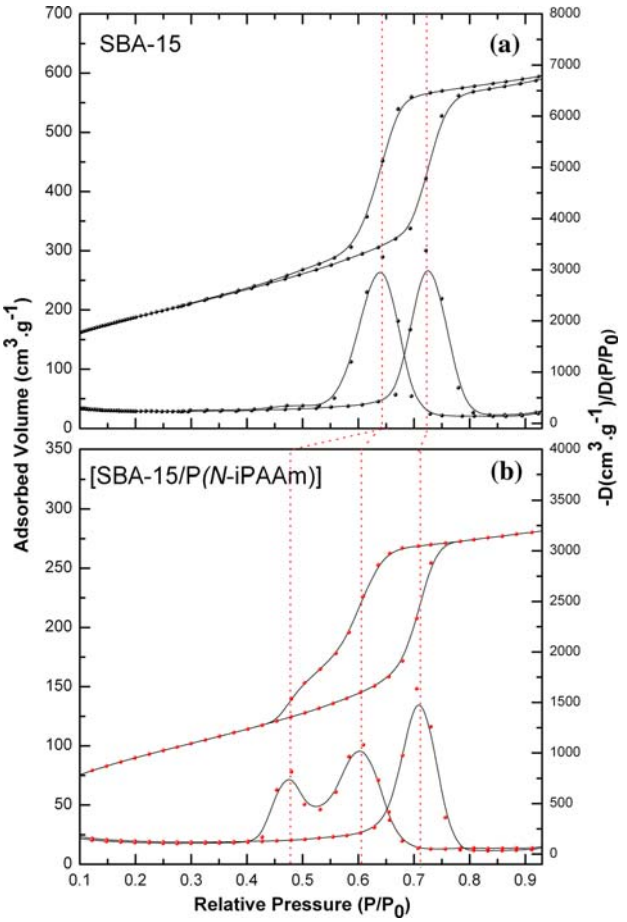

Fig. 1 N_2 adsorption–desorption isotherms and respective derived curves of **a** SBA-15 and **b** [SBA-15/P(*N*-iPAAm)]

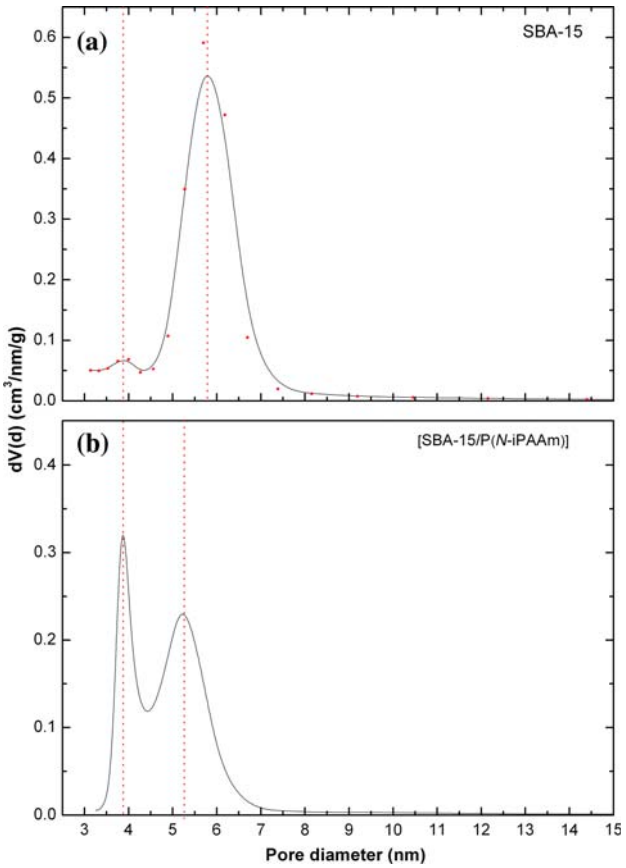

Fig. 2 Pore size distribution of **a** SBA-15 and **b** [SBA-15/P(*N*-iPAAm)]

is delayed until the capillary evaporation from the constrictions take place [28, 29]. This behaviour is often referred to as a pore blocking phenomenon and is attributed to the formation of porous plugs in the ordered channels of SBA-15. After polymerization, the shape of the hysteresis loop in the N_2-sorption isotherm displays a broadening suggestive of a reduction in pore size uniformity [24].

Indeed, the desorption branch shifted towards lower relative pressure P/P_0 with a concurrent decrease in the pore diameters. Such a decrease can be verified by analysing the inflection points of the desorption isotherms and the pore size distribution graphs (Fig. 2). The desorption isotherm of mesoporous silica presented an inflection point of 0.64 at P/P_0. On the other hand, the hybrid sample presented two inflections point of 0.60 and 0.47 around P/P_0; this means that the presence of an organic phase in the silica matrix provoked a shift to a smaller relative pressure related to a decrease in pore size [27].

The adsorption isotherms obtained after atenolol incorporation into the pores of SBA-15 and [SBA-15/P(*N*-iPAAm)] still displayed a mesoporous characteristic (data not shown). The loading degrees for these samples was 18 wt% for the SBA-15 and 17 wt% for [SBA-15/P(*N*-iPAAm)], according to the TGA results, which resulted in decreases in surface area of approximately 46 wt% and 59% for SBA-15 and the hybrid sample, respectively.

Figure 3a shows the FTIR spectra of all the studied samples. The spectra of pure SBA-15 and the hybrid sample exhibited different absorption bands. The spectrum of SBA-15 is dominated by ν_{O-H} modes, presenting a broad and intense band at 3440 cm^{-1} assigned to hydroxyl groups. A broad and very intense band in the range 1000–1200 cm^{-1} corresponding to $\nu_{Si-O-Si}$ modes of the siliceous matrix of SBA-15 is also present. In hybrid systems, the bands corresponding to the ν_{C-H} modes of P(*N*-iPAAm) are observed at 2972–2875 cm^{-1}; the bands attributed to isopropyl group are located at 1386 and 1368 cm^{-1}; the band corresponding to the bending vibration of CH_3 is located at 1456 cm^{-1}, whereas the bands arising from C=O stretching and N–H bending vibrations are observed at 1645 and 1550 cm^{-1}, respectively.

The monomer characteristic bands (νC=C 1620 cm^{-1}, δCH_2 = 1409 cm^{-1}, δH_2C=C– 1305 and 1325 cm^{-1}, δvinyl group at 990 and 916 cm^{-1}) are not present in the

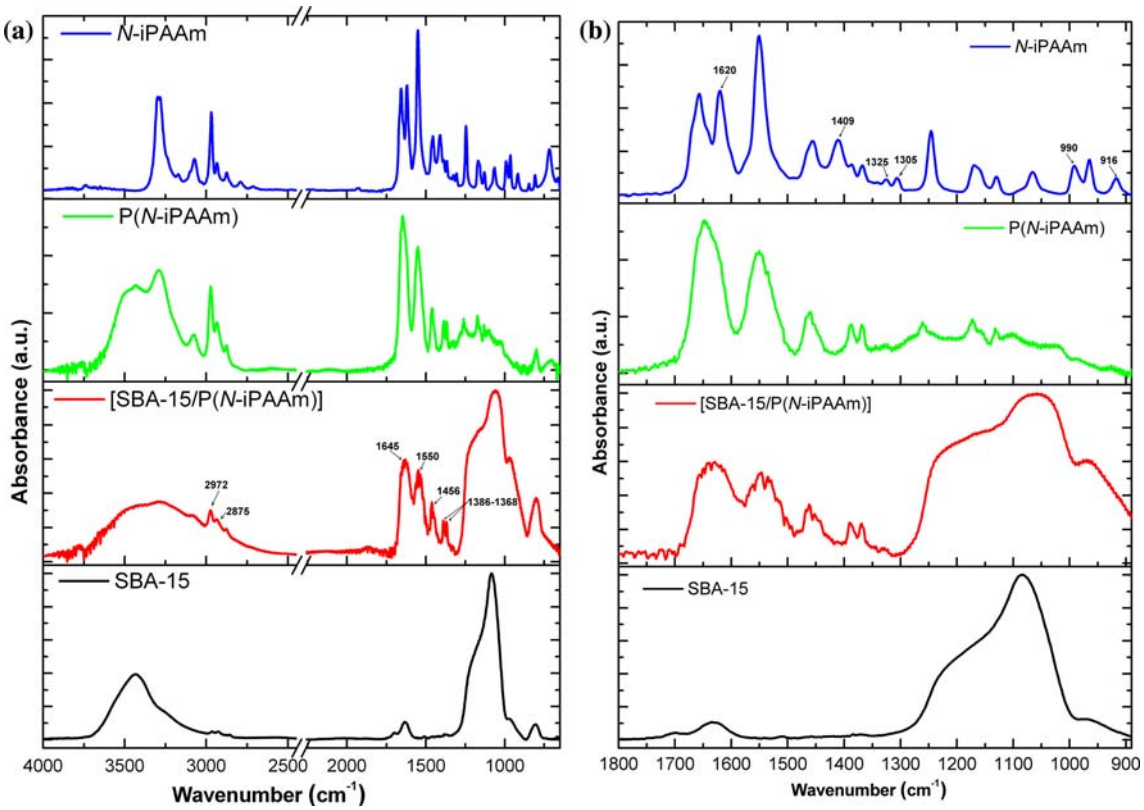

Fig. 3 **a** FTIR spectra of *N*-iPAAm, P(*N*-iPAAm), [SBA-15/P(*N*-iPAAm)] and SBA-15. **b** Expanded spectra in the range 1800–900 cm^{-1}

hybrid sample spectra, as can be seen in the scale-expanded FTIR spectrum in the 1800–900 cm^{-1} region (Fig. 3b). These results prove the presence of P(*N*-iPAAm) in SBA-15 pores with no other significant synthesis components (monomer, initiator or accelerator) and demonstrate the successful conversion of the monomers into polymer. The presence of the drug in the mesoporous material was also confirmed by FTIR. The FTIR spectra of pure SBA-15 and SBA-15/atenolol exhibited different absorption bands. Comparing the scale-expanded FTIR spectrum of SBA-15 with that of the impregnated material in the 1800–1300 cm^{-1} region (Fig. 4), it can be observed that some characteristic stretching and bending vibrations present in the atenolol spectrum, such as 1398, 1384, 1460, 1514, 1583, 1614 and 1660 cm^{-1}, are observed in the SBA-15-atenolol FTIR spectrum in lower intensities, probably as a result of the limited capacity of incorporation of the drug into the mesopores. Similar results were observed for the hybrid sample containing atenolol. However, we did not observe all characteristic vibrations of the atenolol molecule, because some vibration modes of atenolol occurred in the same frequency interval of the P(*N*-iPAAm) modes (Fig. 4).

The amount of polymer loaded in the SBA-15 host was determined by thermogravimetry. The TGA curves of all the systems are shown in Fig. 5. The weight losses of SBA-15, the polymer and the hybrid were evaluated in the range 273–973 K and are shown in Table 2. The TGA pattern of SBA-15 demonstrates one weight loss around 13.0% from environment temperature to 423 K that was attributed to the thermodesorption of physically adsorbed water. Above of this temperature and up to 773 K, no significant weight loss is verified. In this temperature range, a small weight loss of approximately 1.3% was attributed to the decomposition of residual triblock copolymer. In case of the P(*N*-iPAAm) and the hybrid sample, weight loss occurred in three distinct regions. The first region goes from ambient temperature to 773 K, with a weight loss of about 11.6% for P(*N*-iPAAm) and the hybrid sample that might be due to the loss of residual water present in the structure of these materials. The second region for P(*N*-iPAAm) and the hybrid sample occurs in the temperature range between 573 and 773 K, corresponding to 81.9 and 27.0% of the respective initial masses. It may be associated with the degradation of the polymer chains. The third and last region for P(*N*-iPAAm) and the hybrid sample occurs in the range from 573 to 773 K and corresponds to 1.8 and 5.2%, of the respective initial masses, which may be associated with the degradation of the remaining polymeric chains.

The SEM images of mesoporous SBA-15 particles before and after formation of P(*N*-iPAAm) are shown in

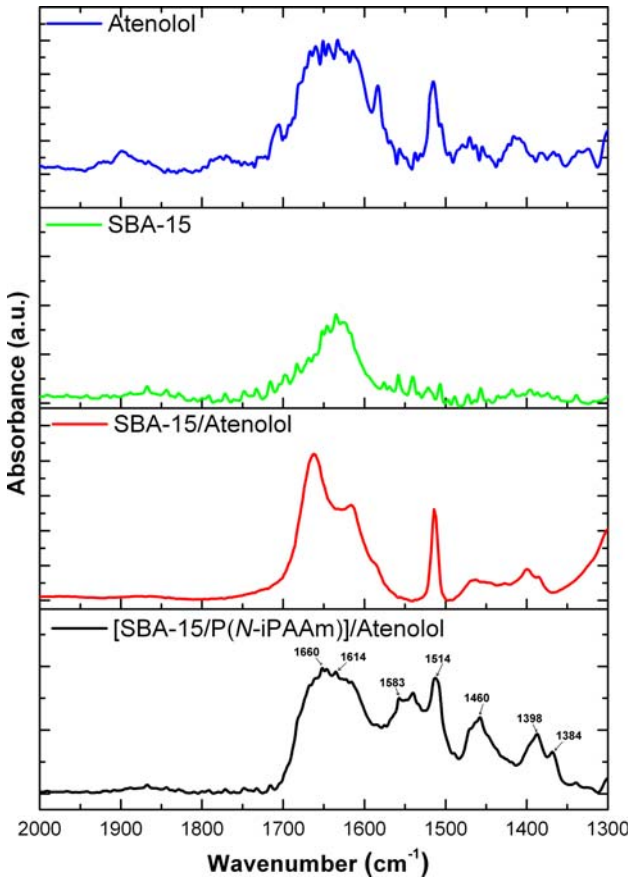

Fig. 4 FTIR expanded spectra of atenolol, SBA-15, SBA-15/atenolol and [SBA-15/P(*N*-iPAAm)]/atenolol

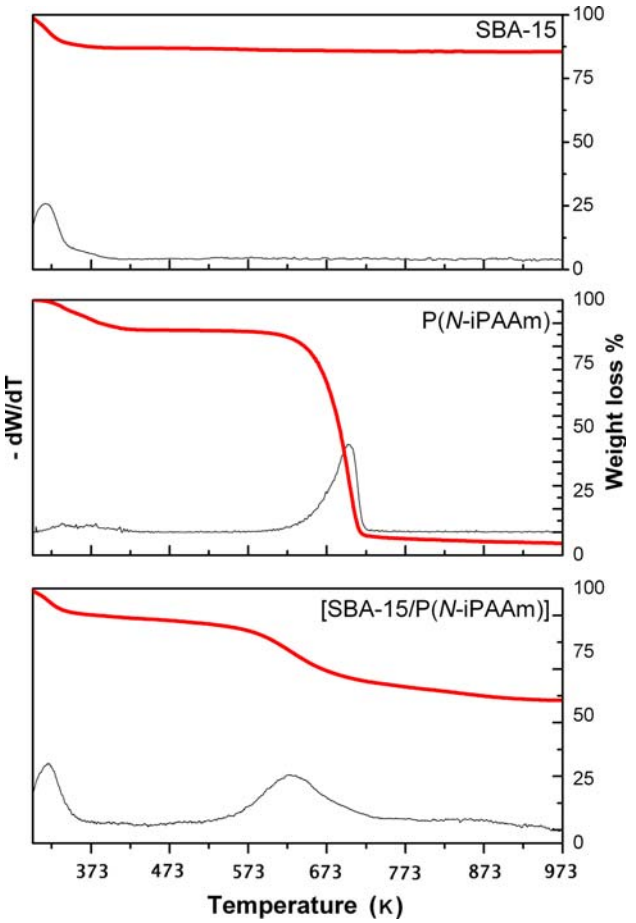

Fig. 5 TGA curves of P(*N*-iPAAm), [SBA-15/P(*N*-iPAAm)] and SBA-15

Fig. 6a, b, respectively. The SEM images of SBA15 evidence the presence of elongated, vermicular-shaped particles 590 nm wide. SBA-15 consists of many rope-like domains with average sizes of 1.7 μm aggregated into wheat-like macrostructures. A similar morphology is observed after the polymerization of P(*N*-iPAAm) inside the SBA-15 network, presenting 450 nm width.

TEM images of SBA-15 after the polymerization of P(*N*-iPAAm) into the silica network are shown in Fig. 7. A well-defined hexagonal arrangement of uniform pores was observed when the electron beam was parallel to the main axis of the mesopores (Fig. 7a, b) along [100] direction when the electron beam was perpendicular to the main axis. Thus, the TEM investigation gives consistent evidence that the ordered structure is preserved in the approach proposed in this study to obtain hybrid system. The hybrid structures obtained do not present distinct TEM images when compared to pure SBA-15, in our previous work [9]. This fact may be attributed to poor contrast in the TEM measurement of polymerized P(*N*-iPAAm) with regard to the SBA-15 matrix, which made the visualization of this structure by TEM difficult.

Table 2 TGA of SBA-15, P(*N*-iPAAm) and [SBA-15/P(*N*-iPAAm)]

Sample	Weight loss (%)			Residues (%)
Temperature (K):	298–423	573–773	773–973	
SBA-15	13.0	1.30	–	85.7
P(*N*-iPAAm)	11.6	81.9	1.80	4.70
[SBA-15/P(*N*-iPAAm)]	11.6	27.0	5.20	56.2

Drug release

Atenolol, a known beta-adrenoceptor antagonist, is used to treat hypertension because of its ability to dilate blood vessels and allow blood to flow under lower pressure, and was used to study thermosensitive drug release by hybrid silica-P(*N*-iPAAm) nanoporous materials. Drug loading was determined through UV–Vis analysis in SBF solution by measuring the absorbance of atenolol at 274 nm, as reported in Ref. [11]. The cumulative amount of atenolol released as a function of time from the tested materials are given in

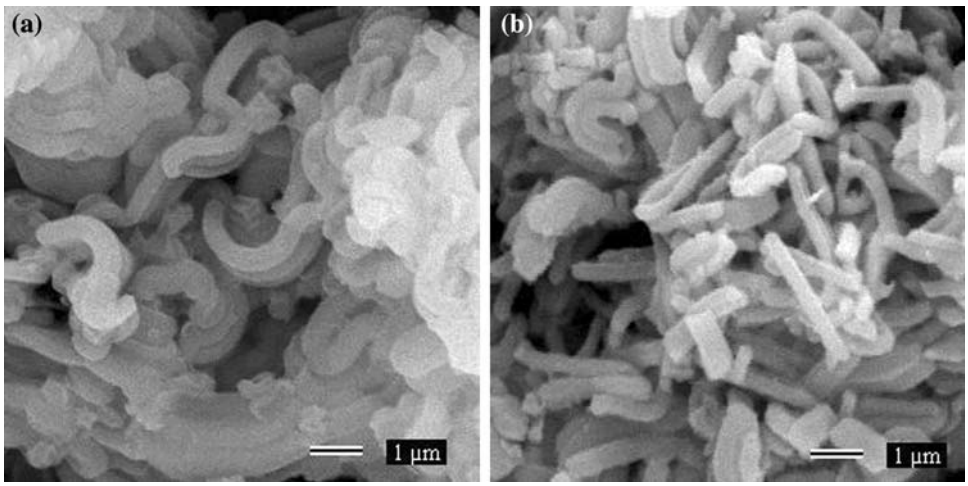

Fig. 6 SEM micrographs of **a** SBA-15 and **b** [SBA-15/P(*N*-iPAAm)] hybrid samples

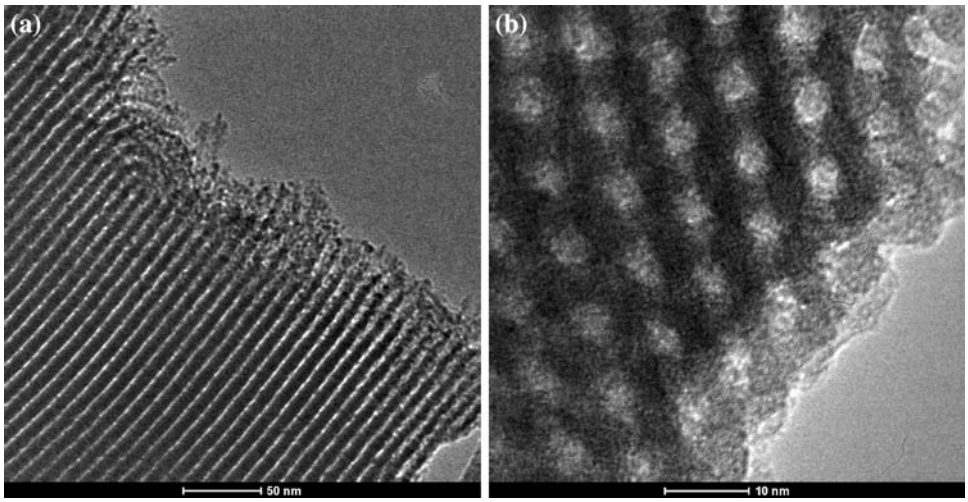

Fig. 7 TEM images of [SBA-15/P(*N*-iPAAm)] **a** viewed along the pore axis and **b** perpendicularly to the pore axis

Fig. 8a, b, whereas the cumulative drug release profiles plotted against time together with the temperature are presented in Fig. 8c. In this figure, the discontinuity in the release profile of the hybrid system as a function of temperature is clearly observed (indicated by arrows above the respective curves). This response in the hybrid system is a great indicative of the polymer phase behaviour. A quasi-linear behaviour in the release profile of SBA-15 as a function of temperature is also displayed in Fig. 8c. All in vitro studies were performed under continuous flow conditions.

As expected, the release of atenolol from pure SBA-15 is temperature dependent (Fig. 8a). This behaviour can be explained considering that the overall drug delivery into the medium is controlled by diffusion through the porous channels. However, as shown by the release profile, delivery seems to be less effective at temperatures as low as 283 K, since this system present comparatively smaller delivery rate at this temperature. In this case, the drug was trapped into the porous structures of the silica network, which may be explained by two simultaneous behaviours: the diffusion rate in the mesoporous material is severely affected at this temperature, and the drug interacts with the mesoporous silica through hydrogen bonds due to the affinity of functional groups amine, amide and hydroxyl of the atenolol molecules and the silanol groups present in the mesoporous silica, as ascribed by the relatively polar hydrophilic character of the drug. At this temperature (283 K), the thermodynamic conditions are not enough to destabilize the hydrogen interactions between the hydrophilic groups of the drug and the silanol groups of silica. In this way, atenolol presents a tendency to remain in the silica nanostructure. When the temperature was raised to 298 K, the interactions between the drug molecules and the silica surface are affected, causing its rupture and a major release of atenolol to the medium. At 313 K, this phenomenon holds on indeed and it is more evident as demonstrated by the release profile in Fig. 8a.

The analysis of the performance of the hybrid system as a drug delivery device (Fig. 8b) shows that the release profiles of silica-P(*N*-iPAAm) varies with temperature,

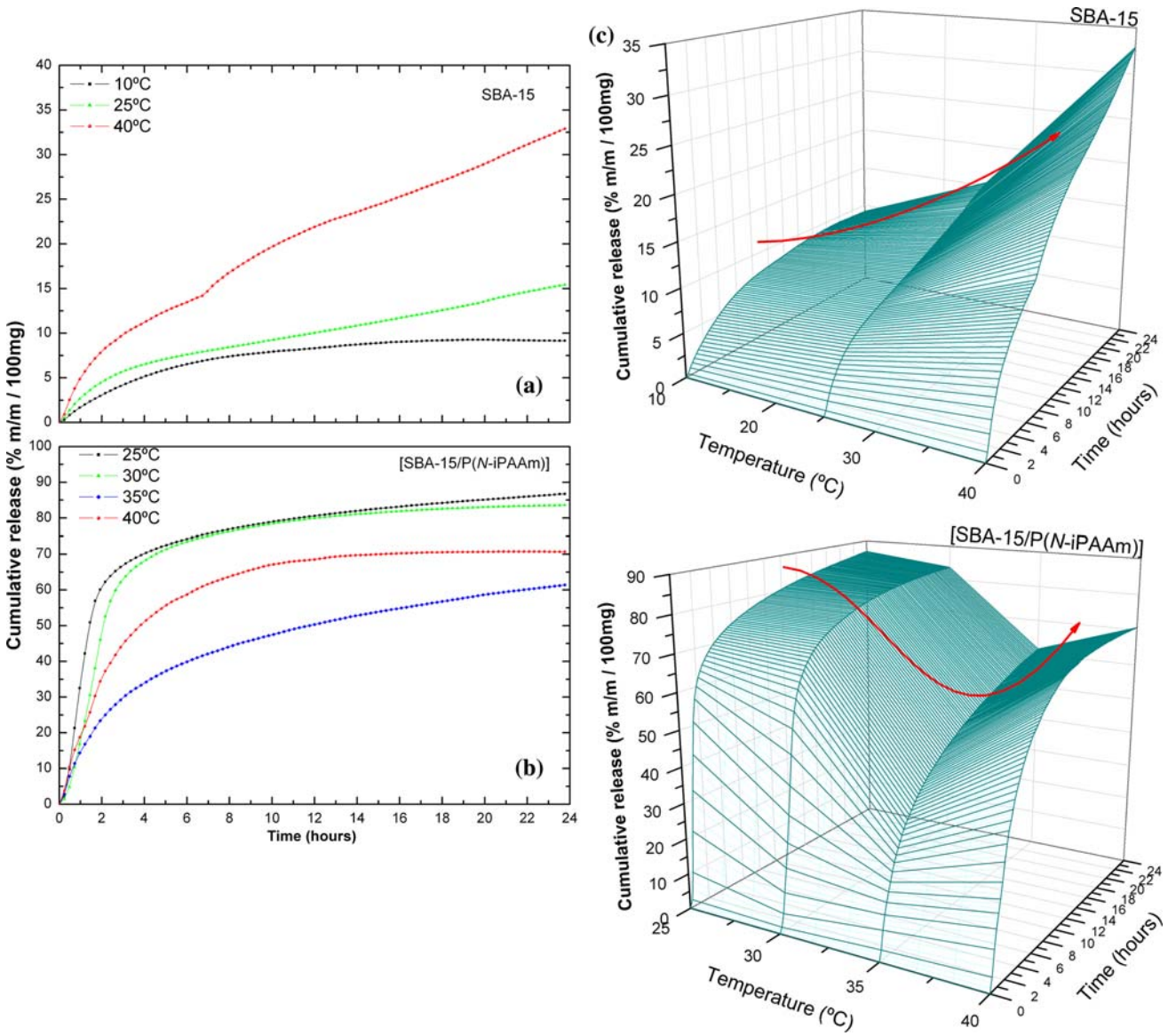

Fig. 8 **a**, **b** Cumulative release profile of atenolol from SBA-15 and [(SBA-15)/P(*N*-iPAAm)] at different temperatures and **c** cumulative release profile of atenolol plotted against time and temperature for SBA-15 and [(SBA-15)/P(*N*-iPAAm)]

when compared to that of pure SBA-15. At 298 K, the release rate was high, followed by a sustained release rate; a similar behaviour was observed at 303 K. However, when the temperature was increased to and maintained at 313 K, a slower and sustained release rate was observed. Nevertheless, it rapidly decreased when the temperature was reduced to 308 K. The behaviour shown in Fig. 8b suggests that other factors besides temperature affect drug release. These observations lead us to suggest that the drug release response of hybrid systems depends on temperature and the polymer phase behaviour. The LCST of P(*N*-iPAAm) is around 306 K; when the temperature was lower than the LCST, the polymer swelled and drug release was faster. When the temperature was above the LCST, the polymer collapsed, acting as a diffusion barrier and the drug release from the pores was significantly blocked. With the increase in temperature, an increase in drug diffusion would be expected; however, the increase in temperature provokes a contraction of the polymer network in the hybrid nanostructure. This contraction creates a physical barrier to the drug diffusion, thus decreasing its release to the medium. This temperature-dependent behaviour becomes critical upon the complete collapse of the polymer chains at around 306 K, when the structure barrier to diffusion is the largest. This fact explains the great reduction in the release rate of atenolol from the hybrid system from 298 and 303 K to 308 K. Above the LCST, the polymer does not present phase change anymore, remaining

contracted without structural variation. The effect of temperature is illustrated in Fig. 8b, when it varies from 308 to 313 K, presenting larger release of atenolol. Even though the release rate is large at this temperature, it is lower than at 298 and 303 K, as the polymer expanded and consequently presented a lesser barrier to the diffusion of atenolol. Therefore, below the LCST, the contraction phenomenon of the polymeric framework in the silica exerts a major influence than the temperature on the release of atenolol to the medium. Above the LCST, the conformational aspect of the polymer does not affect the process and the temperature becomes the dominant variable in the release process. Similar results were presented by other authors. You et al. [16] demonstrate that the phase state of a temperature-responsive polymer can control opening and closing of the pores when grafted onto preformed micro-to-mesoporous silica nanoparticles. The resulting nanoparticle–polymer composites show uptake and release of fluorescein at room temperature (below the LCST, of the polymer) and at 311 K, the entrances of pores are blocked by the collapsed PNIPAM chains, and the release of fluorescein from the voids of system is significantly obstructed. In previous study, Satarkar and Hilt [30] suggested that the suppression of the release in systems is speculated to be a result of collapse of the hydrogel network with heating above LCST.

The above results show that the composition and morphology of carrier materials and temperature are important factors in drug delivery. Although important, these conclusions are preliminary and a deeper study of drug release kinetics employing adequate mathematical modelling of the system with different amounts of organic phase in the SBA-15 matrix as a function of temperature is planned for future work.

Conclusion

Summarizing, we developed an easy and direct synthesis route to obtain hybrid functional nanosystems based on silica-P(*N*-iPAAm) using a neutral surfactant without any functionalization method. The applicability of this hybrid system as a matrix for controlled drug delivery was studied to establish the influence of temperature on atenolol release. The results indicate that the silica-P(*N*-iPAAm) hybrid-ordered mesopores have a potential to encapsulate bioactive molecules. The incorporation of the polymer phase in mesoporous silica led to a significant change in the structural properties of the system without destroying the ordered hexagonal structure of SBA-15 shown by TEM images. However, the surface area, pore size and volume of the hybrid system decreased due to the introduction of the polymer. Moreover, the thermosensibility of P(*N*-iPAAm) was retained in the hybrid system, which had a low critical solution temperature, similar to that of pure P(*N*-iPAAm). The response of this hybrid system as a drug delivery device is influenced by volumetric contraction of P(*N*-iPAAm) up to the LCST due to phase transition; above LCST, the drug release depends essentially on the temperature.

Acknowledgement This study has been supported by CAPES, CNPq and FAPEMIG.

References

1. Hamley IW (2003) Nanotechnology 14:39
2. Soler-Illia GJAA, Sanchez C, Lebeau B, Patarin J (2002) Chem Rev 102:4093
3. Paul W, Sharma CP (2006) Am J Biochem Biotechnol 2:41
4. Rusu VM, Ng CH, Wilke M, Tiersch B, Fratzl P, Peter MG (2005) Biomaterials 26:5414
5. Davis ME (2002) Nature 417:813
6. Taguchi A, Schuth F (2005) Microporous Mesoporous Mater 77:1
7. Izquierdo-Barba I, Colilla M, Vallet-Regí M (2008) J Nanomater 3:1
8. Sousa A, Souza KC, Reis SC, Sousa RG, Windmöller D, Machado JC, Sousa EMB (2008) J Non-Cryst Solids 354:4800
9. Sousa A, Souza KC, Sousa EMB (2008) Acta Biomater 4:671
10. Wan Y, Shia Y, Zhao D (2007) Chem Commun 897
11. Sousa A, Sousa EMB (2006) J Non-Cryst Solids 352:3451
12. Geever LM, Nugent MJD, Higginbotham CL (2007) J Mater Sci 42:9845. doi:10.1007/s10853-007-1814-4
13. Lee WF, Lin YH (2006) J Mater Sci 41:7333. doi:10.1007/s10853-006-0882-1
14. Freitas RFS, Cussler EL (1987) Chem Eng Sci 42:97
15. Sousa RG, Prior-Cabanillas A, Quijada-Garrido I, Barales-Rienda JM (2005) J Controlled Release 102:595
16. You YZ, Kalebaila KK, Brock SL, Oupicky D (2008) Chem Mater 20:3354
17. Zhou Z, Zhu S, Zhang D (2007) J Mater Chem 17:2428
18. Zhu S, Zhou Z, Zhang D, Jin Li Z (2007) Microporous Mesoporous Mater 106:56
19. Chang JH, Kim KJ, Shin Y-K (2004) Bull Korean Chem Soc 25:1257
20. Zhao D, Huo Q, Feng J, Chmelka BF, Stucky GD (1998) J Am Chem Soc 120:6024
21. Sousa RG, Magalhães WF, Freitas RFS (1998) Polym Degrad Stab 61:275
22. Sing KSW, Everett DH, Haul RAW, Moscou L, Pierotti RA, Rouquerol J, Siemieniewska T (1985) Pure Appl Chem 57:603
23. Sayari A, Liu P, Kruk M, Jaroniec M (1997) Chem Mater 9:2499
24. Gregg SJ, Sing KSW (1982) Standard data for alpha-s method comment, 2nd edn. p. 93
25. Cheng Q, Pavlinek V, Lengalova A, Li C, He Y, Saha P (2006) Microporous Mesoporous Mater 93:263
26. Choi M, Kleitz F, Liu D, Lee HY, Ahn W-S, Ryoo R (2005) J Am Chem Soc 127:1924
27. Kruk M, Jaroniec M, Joo SH, Ryoo R (2003) J Phys Chem B 107:2205
28. Kruk M, Jaroniec M (2001) Chem Mater 13:3169
29. Kruk M, Jaroniec M, Sayari A (1997) Langmuir 13:6267
30. Satarkar NS, Hilt ZJ (2008) Acta Biomater 4(1):11